Nanophononic Metamaterial: Thermal Conductivity Reduction by Local Resonance

Bruce L. Davis and Mahmoud I. Hussein*
Department of Aerospace Engineering Sciences, University of Colorado Boulder, Boulder, Colorado 80309, USA
(Received 24 June 2013; published 7 February 2014)

We present the concept of a locally resonant nanophononic metamaterial for thermoelectric energy conversion. Our configuration, which is based on a silicon thin film with a periodic array of pillars erected on one or two of the free surfaces, qualitatively alters the base thin-film phonon spectrum due to a hybridization mechanism between the pillar local resonances and the underlying atomic lattice dispersion. Using an experimentally fitted lattice-dynamics-based model, we conservatively predict the metamaterial thermal conductivity to be as low as 50% of the corresponding uniform thin-film value despite the fact that the pillars add more phonon modes to the spectrum.

DOI: 10.1103/PhysRevLett.112.055505 PACS numbers: 63.22.-m, 65.40.-b, 84.60.-h

The utilization of nanostructured materials for control of heat transport is a rapidly growing area of research [1]. Specifically, the manipulation of heat carrying phonons, or elastic waves that propagate and scatter at the nanoscale, can yield beneficial thermal properties. One pivotal application relates to thermoelectric materials, or the concept of converting energy in the form of heat into electricity and vice versa. The ability to use nanostructuring to reduce the thermal conductivity k without negatively impacting the power factor $S^2\sigma$ (where S is the Seebeck coefficient and σ is the electrical conductivity) provides a promising avenue for achieving high values of the thermoelectric energy conversion ZT figure of merit [2].

The manipulation of elastic waves in a periodic medium can be realized primarily in two distinct ways: (i) the utilization of Bragg-scattering phononic crystals and (ii) the introduction of local resonance. The latter, which is proposed here for the first time for the reduction of the thermal conductivity, renders the medium a "metamaterial." The concept of a phononic crystal [3] involves a material with an artificial periodic internal structure for which the lattice spacing has a length scale on the order of the propagating waves. In such a configuration, wave interferences occur across the unit cell providing a unique frequency band structure with the possibility of band gaps. Focusing on nanoscale phonon transport, the periodic material can be realized in a variety of ways such as by the layering of multiple constituents, also known as a layered superlattice [4], or the introduction of inclusions and/or holes, as in a nanophononic crystal (NPC) [5]. The concept of a metamaterial, on the other hand, generally involves the inclusion of local resonators which enable unique subwavelength properties to emerge. While periodicity is advantageous, it is not necessary in a metamaterial. At the macroscale (where the focus is on acoustics or mechanical vibrations), periodic locally resonant metamaterials have been considered in various forms, such as by having heavy inclusions coated with a compliant material (e.g., rubber-coated lead spheres) and hosted in a relatively lighter and less stiff matrix (e.g., epoxy) [6], or by the presence of pillars on a plate [7].

In this Letter, we introduce the concept of a phononic metamaterial at the nanoscale, which we refer to as a nanophononic metamaterial (NPM). The goal is to significantly reduce the thermal conductivity in a nanostructured semiconducting material and to do so without affecting other important factors, especially the electrical conductivity. For both functional and practical purposes, we choose silicon thin films as the foundation material for the creation of a locally resonant NPM. Using a reduced-dimension material such as a thin film already causes a reduction of k of up to an order of magnitude [8] without necessarily impacting $S^2\sigma$ [9], and is also favorable from the point of view of device integration. The choice of silicon is beneficial due to its wide use in the electronics industry and ease of fabrication; however, other materials may be considered in the future. The resonators take the form of a periodic array of nanoscale pillars that extrude off the surface of the thin film (on either one side or both sides, as practically permitted). Such structure has been considered in the literature for other applications and shown to be feasible from the point of view of fabrication using techniques such as dry etching [10] and metal assisted chemical (wet) etching [11]. The primary advantage of this configuration is that the pillars exhibit numerous local resonances that couple, or more specifically, hybridize with the underlying atomic-level phonon dispersion of the thin film and does so across the full range of its spectrum. These couplings drastically lower the group velocities (at the locations where the hybridizations take place) and, consequently, the thermal conductivity. This phenomenon is also known as avoided crossing, which has been studied in naturally occurring materials that have guest atoms encapsulated in caged structures such as clathrates [12]. In contrast to a NPM, however, the hybridizations in these systems are limited to the modes of the guest atom and

typically take place only across a narrow band within the acoustic range of the spectrum. Another important benefit to utilizing pillars is that the feature manipulating the group velocities (i.e., the pillar itself) is physically outside of the primary flow path of the electrons (which resides in the main body of the thin film). This is a key advantage compared to thin-film-based NPCs, in which the inclusions or the holes penetrate through the thickness of the thin film and, hence, may undesirably cause an obstruction to the electron transport in addition to scattering the phonons. Furthermore, the concern about the competition between coherent and nanofeature-induced incoherent thermal transport is no longer of critical importance because the local resonances are phase independent. This quality provides yet another practical benefit as it frees the NPM from restrictions on geometric tolerances.

We begin our investigation with the creation of an atomic-level unit cell model for a uniform silicon thin film with thickness t. We resort to a conventional cell (CC) description which consists of eight atoms packaged as a cube with side length $a = 0.54$ nm. Because of this conveniently shaped boxlike structure, the CC will be used as our building block which we will replicate along an orthogonal simple cubic lattice to generate a supercell for the thin-film structure. This is done for the uniform thin film and will be built upon later when a pillar is added to the free surface(s). For the uniform thin film, the supercell consists of a vertical strip constructed by stacking M CCs on top of each other along the out-of-plane z direction. The dimensions of this supercell will be denoted by $A_x \times A_y \times A_z$, where $A_x = A_y = a$ and $A_z = Ma = t$.

We obtain the full phonon band structure for a set of suspended uniform silicon thin films by running atomic-scale lattice dynamics (LD) calculations in which the three-body Tersoff potential [13] is used for the Si-Si bonds with only the first nearest neighboring interactions considered. All calculations are conducted after minimizing the interatomic potential energy at constant pressure. For the thermal conductivity predictions, we use the Callaway-Holland (C-H) model [14] which is expressed as

$$k = \frac{1}{A_z \pi} \sum_{\lambda} \int_0^{\pi/A_x} C(\kappa,\lambda) v_g^2(\kappa,\lambda) \tau(\kappa,\lambda) \kappa d\kappa \qquad (1)$$

along the x-direction-aligned ΓX path, where κ, λ, C, v_g, and τ denote the phonon wave number, branch index, specific heat, group velocity, and scattering time, respectively. The three latter quantities are dependent on the phonon dispersion. The specific heat is expressed as $C(\kappa,\lambda) = k_B[\hbar\omega(\kappa,\lambda)/k_B T]^2 f(\kappa,\lambda)$, where $f(\kappa,\lambda) = e^{\hbar\omega(\kappa,\lambda)/k_B T}/[e^{\hbar\omega(\kappa,\lambda)/k_B T} - 1]^2$, ω is the frequency, T is the temperature, k_B is the Boltzman constant, and $\hbar$ is the reduced Plank's constant. The group velocity is expressed as $v_g(\kappa,\lambda) = \partial\omega(\kappa,\lambda)/\partial\kappa$ and the scattering time as $\tau(\kappa,\lambda) = [\tau_U(\kappa,\lambda)^{-1} + \tau_I(\kappa,\lambda)^{-1} + \tau_B(\kappa,\lambda)^{-1}]^{-1}$, where $\tau_U^{-1}(\kappa,\lambda) = AT\omega^2(\kappa,\lambda)e^{-B/T}$, $\tau_I^{-1}(\kappa,\lambda) = D\omega^4(\kappa,\lambda)$, and $\tau_B^{-1}(\kappa,\lambda) = |v_g|/L$, representing umklapp, impurity, and boundary scattering, respectively. The parameters A, B, and D are all obtained empirically. For A and B, we utilize measured data for uniform silicon thin films on a subtrate [8] since the temperature-dependent trends are similar to their suspended counterparts. Concerning impurity scattering, we use $D = 1.32 \times 10^{-45}$ s^3 [15]. The effective boundary scattering length L is defined as $L = t/(1-p)$, where p is a surface specularity parameter ($0 \le p \le 1$) [1,15]. Because of the high sensitivity of the fitting parameters to the thin-film thickness (especially for very low t), we fit our model for a variety of thicknesses, $t = 20$, 30, 50, 100, 420 nm, around a temperature of $T = 300$ K [16].

We now turn to the main focus of this work which is to determine how the presence of nanoscale resonating pillars reduces the thermal conductivity in a thin film. For a proof of concept, we first consider a problem where the thin-film thickness is extremely small. The baseline study for this case consists of a thin-film supercell with a square base of 6×6 CCs ($A_x = A_y = a_{\mathrm{NPM}} = 3.26$ nm) and a thickness of $M = 5$ CCs ($A_z = t = 2.72$ nm); this corresponds to a rectangular solid containing 1440 atoms. The pillar is placed at the top of the thin film and has a square base of 2×2 CCs (side length of $d = 1.09$ nm) and a height of 3 CCs ($h = 1.63$ nm) and itself contains 96 atoms. The geometrical configuration of both supercells is shown in the insets of Fig. 1(a). The phonon dispersion along the ΓX path is presented in the same figure for both the uniform thin film and the pillared thin film. For the thermal conductivity predictions, we keep the umklapp scattering parameters constant between the uniform and pillared cases. This provides a conservative approximation for the latter since it has been shown that avoided crossings cause a slight reduction of phonon lifetimes [12]. We also keep the boundary scattering parameters constant since the pillars are relatively small in the cross-sectional area and are external to the main cross section of the nominal thin film; and they are, therefore, not expected to cause a significant deviation from the uniform thin-film boundary scattering parameters. For the present model, we use appropriately fitted A and B parameters for a $t = 2.72$-nm thin film using the experimental data in Refs. [8] (see [16] for details) and consider the case of $p = 0$.

The results are presented in Fig. 1, from which we note several observations: (i) The lower (acoustic) branches contribute to a significant portion of the thermal conductivity in both the uniform and pillared thin films. In addition, we see that the higher wave numbers also significantly contribute to the thermal conductivity (contrary to the bulk case). One factor to recall here is that the boundary scattering term has been set to the thin-film thickness, i.e., $L = t = 2.72$ nm. When this value is very small, the long waves (i.e., those near the Γ point in the

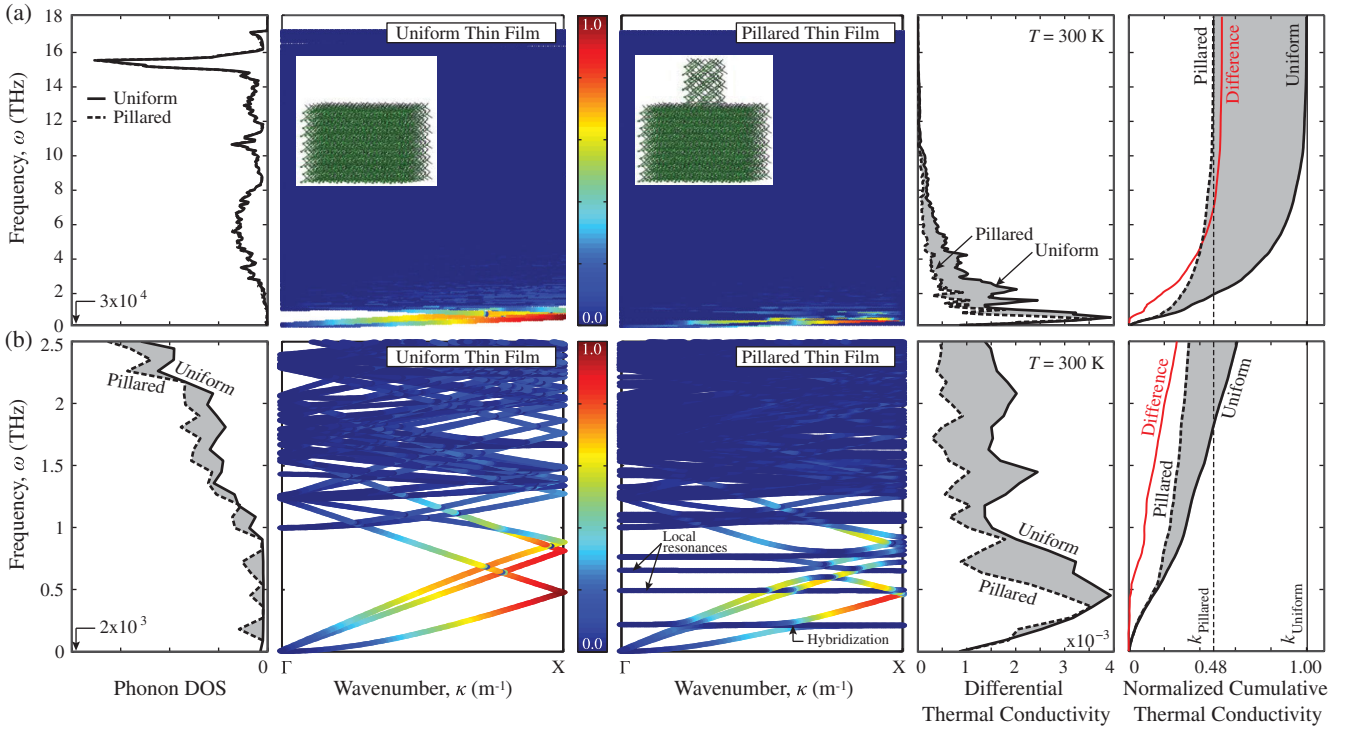

FIG. 1 (color). Comparison of the phonon dispersion and thermal conductivity of a pillared silicon thin film with a corresponding uniform thin film. The dispersion curves are colored to represent the modal contribution to the cumulative thermal conductivity, normalized with respect to the highest modal contribution in either configuration. The full spectrum is shown in (a) and the $0 \leq \omega \leq 2.5$ THz portion is shown in (b). Phonon DOS and the thermal conductivity, in both differential and cumulative forms, are also shown. The gray regions represent the difference in quantity of interest between the two configurations. The introduction of the pillar in the unit cell causes striking changes to all these quantities.

band diagram) are effectively eliminated and, as a result, we get the low contribution at the low wave number end of the acoustic branches. (ii) The presence of the pillars causes a series of flat locally resonant phonon modes to appear across the entire spectrum, i.e., at both subwavelength and superwavelength frequencies. These modes interact with the underlying acoustic and optical thin-film phonon modes and form a hybridization of the dispersion curves. This in turn leads to a flattening of the branches at the intersections and hence a reduction in the group velocities and the thermal conductivity. The introduction of the pillars reduces the thermal conductivity to 48% of that of the uniform thin film. This is a remarkable outcome considering that the pillars introduce 288 new degrees of freedom per unit cell, each of which add one more branch to the summation carried out in Eq. (1). Thus even though more heat carriers are added to the system, less energy is actually carried due to the hybridization mechanism. (iii) We note that the branches under 1.5 THz (mostly acoustic branches) for the uniform case contribute approximately to 40% of the thermal conductivity. The presence of the pillars significantly modifies the relative contribution of these branches, which now contribute to roughly 60% of the thermal conductivity. With the pillars, nearly 70% of the thermal conductivity is accounted for by phonons below 2.5 THz compared to 60% without pillars. For the pillared case, the vast majority of this 70% falls within the range $0.5 < \omega \leq 2.5$ THz. The remaining 30% are mostly accounted for in the range $2.5 < \omega \leq 10$ THz. These results indicate that the flattening effect caused by the numerous local resonances on the dense high frequency optical modes causes the contribution profile to shift downwards, allowing the acoustic and low frequency optical modes to carry more weight. However, at very high frequencies (above 10 THz), the thin-film dispersion curves are already too flat, providing the horizontal resonant branches little opportunity for any noticeable alteration of the group velocities.

For the cases considered thus far, we have modeled the dispersion of the thin film with pillars utilizing atomic-scale LD. However, due to the profound computational intensity associated with solving large complex eigenvalue problems, this type of model is limited to very small sizes (using our current resources, this is roughly on the order of 5 nm in supercell side length). Given that current nanostructure fabrication technology is practically limited to minimum feature sizes roughly an order of magnitude larger, we turn to a continuum-based finite-element (FE) model for our LD calculations, albeit we pay special attention to the FE resolution in terms of the number of elements per CC,

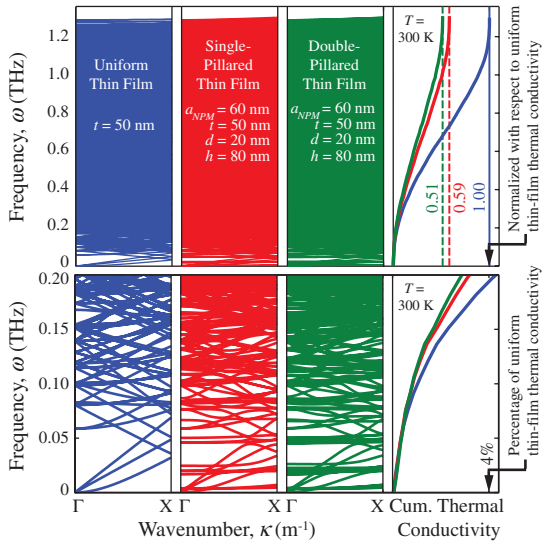

FIG. 2 (color). Full dispersion comparison of a uniform $t = 50$-nm thin film (left), with an 80-nm single pillar (center), and an 80-nm double pillar (right). A focus on the first few dispersion branches is also shown, as well as the cumulative thermal conductivity as a function of frequency.

n_{ele}/CC, when compared to the atomic scale model. To understand the sensitivity of the thermal conductivity prediction to the FE resolution, we include in [16] comparisons of results obtained by both FE and atomic-scale LD models. From these results we note that with increased FE resolution, the FE model maintains a consistent trend and approaches the atomic-scale LD model. We also examine in [16] the FE performance for a larger model (for which atomic-scale LD results are not available) and again observe a converging trend.

Using FE-based lattice dynamics, we now analyze a NPM of a relatively large size: $t = 50$ nm ($A = 6.39 \times 10^{-19}$ s/K, $B = 203$ K, and $p = 0$), $a_{\mathrm{NPM}} = 60$ nm, $d = 20$ nm, and $h = 80$ nm. The room-temperature phonon mean free path in a thin film with a thickness of this order has been suggested to be of the order of a few hundred nanometers [17], thus providing adequate conditions for coherent transport to take effect. We set $n_\kappa = 129$ and $n_{ele}/\mathrm{CC} = 0.109$ for this problem. We also analyse a corresponding uniform thin film for comparison. We again use identical scattering parameters for the uniform and pillared models, noting that this approximation improves with an increase in thin-film thickness. The results appear in Fig. 2 for a NPM with pillars on either one surface or on the two surfaces and for the uniform thin film. We note a few distinctive traits in these results: (i) Consistent with Fig. 1, the maximum frequency between the uniform and pillared cases remains the same despite the extra branches that get introduced due to the added FE degrees of freedom of the pillar, and (ii) despite this addition of degrees of freedom, once again the NPM has a reduced thermal conductivity (59% of the uniform thin film's value) due to the penetration of the local resonance branches into the phonon spectrum. With a higher FE resolution, the predicted reduction is expected to increase (see [16]). As for the double pillared thin film, we observe that additional flat branches appear around the resonant frequencies. This points to a breakage of the degeneracy for the locally resonant modes, which is likely due to a slight asymmetry in the preceding top and bottom surface relaxations. This effect causes further reduction in the thermal conductivity to 51% of the uniform thin film's value. In order to examine the effect of the choice of the umklapp scattering parameters, we repeat these calculations using values for bulk silicon ($A = 2.10 \times 10^{-19}$ s/K and $B = 180$ K; see Davis and Hussein in [5]) and obtain $k_{\mathrm{Pillared}}/k_{\mathrm{Uniform}}$ values of 60% and 54% for the single and doubled pillared thin films, respectively. These numbers are very close to those reported above using the thin-film parameters because at a thickness of $t = 50$ nm, the umklapp scattering behavior approaches that of the bulk material [18]. Finally, we repeat the analysis with a specularity parameter of $p = 1$ and obtain $k_{\mathrm{Pillared}}/k_{\mathrm{Uniform}}$ values of 76% and 73% for the single and doubled pillared thin films, respectively (using recalculated thin-film umklapp scattering parameters, $A = 1.20 \times 10^{-18}$ s/K and $B = 15$ K, which were obtained using $p = 1$).

Locally resonant acoustic metamaterials were introduced by Liu *et al.* [6] to control acoustic waves. Here we have introduced, for the first time, the concept of a locally resonant NPM to control heat waves. In acoustics, the local resonances couple with the dispersion curves associated with the periodic arrangement of the resonators, or the long wave linear dispersion of the embedding medium when looking only at the subwavelength regime; here the coupling is between the local resonance modes and the atomic-scale dispersion of the underlying crystalline material. Acoustic metamaterials, like their electromagnetic counterparts [19], derive their unique properties at subwavelength frequencies. In NPMs, the local resonances produce desirable effects across the entire spectrum, including the superwavelength regime. Indeed, we saw that despite the injection of additional phonons (associated with the added degrees of freedom of the resonators), the thermal conductivity has been reduced, and this is attributed to the hybridizations taking place at both subwavelength and superwavelength frequencies. This outcome provides a broader perspective to the definition of a metamaterial. Finally, our proposed NPM configuration—being based on pillared thin films—provides a powerful mechanism for reducing the thermal conductivity without altering the base thin-film material (e.g., without the insertion of boundary-type scatterers such as holes, inclusions, interfaces, impurities, etc.) and is therefore expected to have a minimal effect on the electrical conductivity. This scenario is markedly advantageous for thermoelectric energy conversion. For our models, we obtained a

conservative prediction of thermal conductivity reduction by as high as a factor of 2 compared to a corresponding uniform thin film. Upon analysis with higher resolution models, optimization of dimensions, exploration of other local resonator geometric configurations, merging of the pillars concept with other thin-film-based thermoelectric materials with proven performances, among other factors, it is perceivable to reach exceedingly high values of ZT using the concept of a nanophononic metamaterial.

The authors would like to thank Dr. E. A. Misawa and the National Science Foundation for support of this research under Grant No. CMMI 0927322, and graduate students L. Liu and O. R. Bilal for their assistance with the FE code programming and mesh setup, respectively.

*mih@colorado.edu

[1] A. A. Balandin and K. L. Wang, Phys. Rev. B **58**, 1544 (1998); G. Chen, Int. J. Therm. Sci. **39**, 471 (2000).

[2] M. S. Dresselhaus, G. Chen, M. Y. Tang, R. G. Yang, H. Lee, D. Z. Wang, Z. F. Ren, J.-P. Fleurial, and P. Gogna, Adv. Mater. **19**, 1043 (2007); G. J. Snyder and E. S. Toberer, Nat. Mater. **7**, 105 (2008).

[3] M. M. Sigalas and E. N. Economou, Solid State Commun. **86**, 141 (1993); M. S. Kushwaha, P. Halevi, L. Dobrzynski, and B. Djafari-Rouhani, Phys. Rev. Lett. **71**, 2022 (1993).

[4] A. N. Cleland, D. R. Schmidt, and C. S. Yung, Phys. Rev. B **64**, 172301 (2001); A. J. H. McGaughey, M. I. Hussein, E. S. Landry, M. Kaviany, and G. M. Hulbert, *ibid.* **74**, 104304 (2006); E. S. Landry, M. I. Hussein, and A. J. H. McGaughey, *ibid.* **77**, 184302 (2008); M. N. Luckyanova, J. Garg, K. Esfarjani, A. Jandl, M. T. Bulsara, A. J. Schmidt, A. J. Minnich, S. Chen, M. S. Dresselhaus, Z. F. Ren, E. A. Fitzgerald, and G. Chen, Science **338**, 936 (2012).

[5] J. N. Gillet, Y. Chalopin, and S. Volz, J. Heat Transfer **131**, 043206 (2009); J. Tang, H.-T. Wang, D. H. Lee, M. Fardy, Z. Huo, T. P. Russell, and P. Yang, Nano Lett. **10**, 4279 (2010); J. K. Yu, S. Mitrovic, D. Tham, J. Varghese, and J. R. Heath, Nat. Nanotechnol. **5**, 718 (2010); P. E. Hopkins, C. M. Reinke, M. F. Su, R. H. Olsson III, E. A. Shaner, Z. C. Leseman, J. R. Serrano, L. M. Phinney, and I. El-Kady, Nano Lett. **11**, 107 (2011); Y. P. He, D. Donadio, J. H. Lee, J. C. Grossman, and G. Galli, ACS Nano **5**, 1839 (2011); B. L. Davis and M. I. Hussein, AIP Adv. **1**, 041701 (2011); J. F. Robillard, K. Muralidharan, J. Bucay, P. A. Deymier, W. Beck, and D. Barker, Chin. J. Phys. (Taipei) **49**, 448 (2011).

[6] Z. Y. Liu, X. X. Zhang, Y. W. Mao, Y. Y. Zhu, Z. Y. Yang, C. T. Chan, and P. Sheng, Science **289**, 1734 (2000).

[7] Y. Pennec, B. Djafari-Rouhani, H. Larabi, J. O. Vasseur, and A.-C. Hladky-Hennion, Phys. Rev. B **78**, 104105 (2008); T. T. Wu, Z. G. Huang, T. C. Tsai, and T. C. Wu, Appl. Phys. Lett. **93**, 111902 (2008).

[8] K. E. Goodson and Y. S. Ju, Annu. Rev. Mater. Sci. **29**, 261 (1999); W. J. Liu and M. Asheghi, Appl. Phys. Lett. **84**, 3819 (2004); J. Appl. Phys. **98**, 123523 (2005).

[9] C. N. Liao, C. Chen, and K. N. Tu, J. Appl. Phys. **86**, 3204 (1999); R. Venkatasubramanian, E. Siivola, T. Colpitts, and B. O'Quinn, Nature (London) **413**, 597 (2001); A. I. Hochbaum, R. Chen, R. D. Delgado, W. Liang, E. C. Garnett, M. Najarian, A. Majumdar, and Y. P., *ibid.* **451**, 163 (2008); A. I. Boukai, Y. Bunimovich, J. Tahir-Kheli, J.-K. Yu, W. A. Goddard III, and J. R. Heath, *ibid.* **451**, 168 (2008).

[10] N. Chekurov, K. Grigoras, A. Peltonen, S. Franssila, and I. Tittonen, Nanotechnology **20**, 065307 (2009).

[11] Z. P. Huang, X. X. Zhang, M. Reiche, L. F. Liu, W. Lee, T. Shimizu, S. Senz, and U. Gosele, Nano Lett. **8**, 3046 (2008).

[12] J. Dong, O. F. Sankey, and C. W. Myles, Phys. Rev. Lett. **86**, 2361 (2001); M. Christensen, A. B. Abrahamsen, N. B. Christensen, F. Furany, N. H. Andersen, K. Lefmann, J. Andreassons, and C. R. H. Bahl, Nat. Mater. **7**, 811 (2008).

[13] J. Tersoff, Phys. Rev. B **38**, 9902 (1988).

[14] J. Callaway, Phys. Rev. **113**, 1046 (1959); M. G. Holland, *ibid.* **132**, 2461 (1963).

[15] N. Mingo, Phys. Rev. B **68**, 113308 (2003).

[16] See Supplemental Material at http://link.aps.org/supplemental/10.1103/PhysRevLett.112.055505 for details on obtaining the thin-film umklapp scattering parameters and for a finite-element resolution analysis of thin-film models.

[17] J. S. Ju and K. E. Goodson, Appl. Phys. Lett. **74**, 3005 (1999).

[18] J. E. Turney, A. J. H. McGaughey, and C. H. Amon, J. Appl. Phys. **107**, 024317 (2010).

[19] J. B. Pendry, A. J. Holden, D. J. Robbins, and W. J. Stewart, IEEE Trans. Microwave Theory Tech. **47**, 2075 (1999); D. R. Smith, W. J. Padilla, D. C. Vier, S. C. Nemat-Nasser, and S. Schultz, Phys. Rev. Lett. **84**, 4184 (2000).